In vivo imaging of middle-ear and inner-ear microstructures of a mouse guided by SD-OCT combined with a surgical microscope

Nam Hyun Cho,[1] Jeong Hun Jang,[2] Woonggyu Jung,[3] and Jeehyun Kim[1,*]

[1] *School of Electrical Engineering, Kyungpook National University, 1370, Sankyuk 3-dong, Buk-gu, Daegu 702-701, South Korea*

[2] *Department of Otorhinolaryngology-Head and Neck Surgery, Kyungpook National University, College of Medicine, 680 Gukchaebosang-ro, Jung-gu, Daegu 700-842, South Korea*

[3] *School of Nano-Bioscience and Chemical Engineering, Ulsan National Institute of Science and Technology 100, Banyeon-ri, Eonyang-eup, Ulju-gun, Ulsan 689-798, South Korea*

[*] *jeehk@knu.ac.kr*

Abstract: We developed an augmented-reality system that combines optical coherence tomography (OCT) with a surgical microscope. By sharing the common optical path in the microscope and OCT, we could simultaneously acquire OCT and microscope views. The system was tested to identify the middle-ear and inner-ear microstructures of a mouse. Considering the probability of clinical application including otorhinolaryngology, diseases such as middle-ear effusion were visualized using *in vivo* mouse and OCT images simultaneously acquired through the eyepiece of the surgical microscope during surgical manipulation using the proposed system. This system is expected to realize a new practical area of OCT application.

OCIS codes: (110.4500) Optical coherence tomography; (170.4940) Otolaryngology; (170.3880) Medical and biological imaging; (170.4500) Optical coherence tomography.

References and links

1. J. W. Casselman, "Diagnostic imaging in clinical neuro-otology," Curr. Opin. Neurol. **15**(1), 23–30 (2002).
2. L. B. Minor, J. P. Carey, P. D. Cremer, L. R. Lustig, S. O. Streubel, and M. J. Ruckenstein, "Dehiscence of bone overlying the superior canal as a cause of apparent conductive hearing loss," Otol. Neurotol. **24**(2), 270–278 (2003).
3. J. E. McClay, R. Tandy, K. Grundfast, S. G. Choi, G. Vezina, G. Zalzal, and A. Willner, "Major and minor temporal bone abnormalities in children with and without congenital sensorineural hearing loss," Arch. Otolaryngol. Head Neck Surg. **128**(6), 664–671 (2002).
4. D. Huang, E. A. Swanson, C. P. Lin, J. S. Schuman, W. G. Stinson, W. Chang, M. R. Hee, T. Flotte, K. Gregory, C. A. Puliafito, and et, "Optical coherence tomography," Science **254**(5035), 1178–1181 (1991).
5. I. Grulkowski, M. Gora, M. Szkulmowski, I. Gorczynska, D. Szlag, S. Marcos, A. Kowalczyk, and M. Wojtkowski, "Anterior segment imaging with Spectral OCT system using a high-speed CMOS camera," Opt. Express **17**(6), 4842–4858 (2009).
6. J. Kim and B. S. Sohn, "Real-time retinal imaging with a parallel optical coherence tomography using a CMOS smart array detector," J. Korean Phys. Soc. **51**, 1787–1791 (2007).
7. T. Gambichler, G. Moussa, M. Sand, D. Sand, P. Altmeyer, and K. Hoffmann, "Applications of optical coherence tomography in dermatology," J. Dermatol. Sci. **40**(2), 85–94 (2005).
8. W. G. Jung, J. Zhang, J. R. Chung, P. Wilder-Smith, M. Brenner, J. S. Nelson, and Z. P. Chen, "Advances in oral cancer detection using optical coherence tomography," Ieee J Sel Top Quant **11**(4), 811–817 (2005).
9. N. H. Cho, U. Jung, H. I. Kwon, H. Jeong, and J. Kim, "Development of SD-OCT for Imaging the in vivo Human Tympanic Membrane," J Opt Soc Korea **15**(1), 74–77 (2011).
10. H. M. Subhash, V. Davila, H. Sun, A. T. Nguyen-Huynh, A. L. Nuttall, and R. K. Wang, "Volumetric in vivo imaging of intracochlear microstructures in mice by high-speed spectral domain optical coherence tomography," J. Biomed. Opt. **15**(3), 036024 (2010).
11. C. T. Nguyen, S. R. Robinson, W. Jung, M. A. Novak, S. A. Boppart, and J. B. Allen, "Investigation of bacterial biofilm in the human middle ear using optical coherence tomography and acoustic measurements," Hear. Res. **301**, 193–200 (2013).

#205660 - $15.00 USD Received 30 Jan 2014; revised 20 Mar 2014; accepted 21 Mar 2014; published 7 Apr 2014

12. C. T. Nguyen, W. Jung, J. Kim, E. J. Chaney, M. Novak, C. N. Stewart, and S. A. Boppart, "Noninvasive in vivo optical detection of biofilm in the human middle ear," Proc. Natl. Acad. Sci. U.S.A. **109**(24), 9529–9534 (2012).
13. B. J. F. Wong, J. F. de Boer, B. H. Park, Z. P. Chen, and J. S. Nelson, "Optical coherence tomography of the rat cochlea," J. Biomed. Opt. **5**(4), 367–370 (2000).
14. B. J. F. Wong, Y. H. Zhao, M. Yamaguchi, N. Nassif, Z. P. Chen, and J. F. De Boer, "Imaging the internal structure of the rat cochlea using optical coherence tomography at 0.827 mu m and 1.3 mu m," Otolaryng Head Neck **130**(3), 334–338 (2004).
15. E. W. Chang, J. T. Cheng, C. Röösli, J. B. Kobler, J. J. Rosowski, and S. H. Yun, "Simultaneous 3D imaging of sound-induced motions of the tympanic membrane and middle ear ossicles," Hear. Res. **304**, 49–56 (2013).
16. S. S. Gao, P. D. Raphael, R. Wang, J. Park, A. P. Xia, B. E. Applegate, and J. S. Oghalai, "In vivo vibrometry inside the apex of the mouse cochlea using spectral domain optical coherence tomography," Biomed. Opt. Express **4**(2), 230–240 (2013).
17. H. M. Subhash, N. Choudhury, F. Y. Chen, R. K. K. Wang, S. L. Jacques, and A. L. Nuttall, "Depth-resolved dual-beamlet vibrometry based on Fourier domain low coherence interferometry," J. Biomed. Opt. **18**(3), 036003 (2013).
18. J. P. Ehlers, Y. K. Tao, S. Farsiu, R. Maldonado, J. A. Izatt, and C. A. Toth, "Integration of a Spectral Domain Optical Coherence Tomography System into a Surgical Microscope for Intraoperative Imaging," Invest. Ophthalmol. Vis. Sci. **52**(6), 3153–3159 (2011).
19. Y. K. K. Tao, J. P. Ehlers, C. A. Toth, and J. A. Izatt, "Intraoperative spectral domain optical coherence tomography for vitreoretinal surgery," Opt. Lett. **35**(20), 3315–3317 (2010).
20. C. Shi, B. C. Becker, and C. N. Riviere, "Inexpensive monocular pico-projector-based augmented reality display for surgical microscope," in *Computer-Based Medical Systems (CBMS), 2012 25th International Symposium on*(IEEE, 2012), pp. 1–6.
21. T. Sielhorst, M. Feuerstein, and N. Navab, "Advanced Medical Displays: A Literature Review of Augmented Reality," J Disp Technol **4**(4), 451–467 (2008).
22. M. Jeon, J. Kim, U. Jung, C. Lee, W. Jung, and S. A. Boppart, "Full-range k-domain linearization in spectral-domain optical coherence tomography," Appl. Opt. **50**(8), 1158–1163 (2011).
23. R. C. Holder, D. J. Kirse, A. K. Evans, T. R. Peters, K. A. Poehling, W. E. Swords, and S. D. Reid, "One third of middle ear effusions from children undergoing tympanostomy tube placement had multiple bacterial pathogens," BMC Pediatr. **12**(1), 87 (2012).

1. Introduction

The otoscope and oto-endoscope as surface imaging modalities are clinically used to diagnose the condition of the TM in an outpatient clinic. Middle-ear and inner-ear structures, which are invisible to the otoscope and oto-endoscope, are evaluated using computed tomography (CT) and magnetic resonance imaging (MRI). These imaging methods are useful diagnostic tools but have limitations such as radiation exposure, low resolution, and high cost. Another currently used method is the surgical microscope, which has the ability to visualize the microstructures of an object [1–3]. During the ear surgery, the use of the microscope is commonly adapted to visualize the surface of TM. As alternative approach to visualize inner structure, optical interferometric imaging has been studied in many fields. The basic principle of OCT is the utilization of the interference effect of a low-coherence light source in near-infrared wavelengths [4]. Further, OCT is an *in vivo* and non-invasive imaging method, and its resolution (1–15 μm) is higher than that of CT and MRI. In addition, OCT provides depth-resolved cross-sectional images by transverse scanning and assembling. OCT imaging technology is mainly applied for diagnosis in ophthalmology and oncology. In particular, OCT has become a commercialized product in ophthalmologic fields and is used to diagnose diseases missed by conventional equipment [5–8]. Recently, imaging studies in otolaryngology using OCT technology have been performed by various research groups all over the world [9–14]. In addition to anatomical studies using an OCT system, functional analyses such as the vibrations of middle-ear structures and the cochlear mechanics of the inner ear have been actively investigated by using optical Doppler tomography (ODT) and laser Doppler Vibrometry (LDV) [15–17].

Middle ear effusion, defined as fluid collection in the middle ear cavity by Eustachian tube dysfunction, and tympanic membrane perforation are common oto-endoscopic findings in patients with otitis media. These findings affect the sound transmission from external auditory canal to cochlea and cause the conductive hearing impairment. In these cases, the depth-resolved cross-sectional imaging of OCT could provide more valuable information than the

#205660 - $15.00 USD Received 30 Jan 2014; revised 20 Mar 2014; accepted 21 Mar 2014; published 7 Apr 2014

imaging of oto-endoscope, such as quantitative estimation of effusion, quality of perforation margin, decision making of surgical intervention by serial change of effusion volume and perforation size. Additionally, middle ear structure including tympanic membrane is an optimal target because OCT probe can visualize this structure directly without blocking by bony structure.

From a surgical perspective, we combined an OCT system with a microscope used in intraoperative imaging. Similar approaches have been reported [18–21], however, most of them are focused on co-registering the field of views of the microscope and the OCT. Surgeon needs to change his/her sight to a computer screen in order to confirm the co-registered images. In this study, we feedback the live OCT images onto the ocular lens of the microscope so that the surgeon can confirm the co-registered images in real time. Therefore, the surgeon has no need to look away from the microscope view to the OCT display so that there is no disruption in the flow of surgery. The efficacy of OCT combined with a surgical microscope in an otolaryngologic area was evaluated by the acquisition of normal middle-ear and inner-ear structures in a mouse. The *in vivo* two-dimensional (2-D) images were obtained from the TM, middle-ear, and inner-ear structures in real-time, and three-dimensional (3-D) images were also reconstructed based on the 2-D images to identify the micro-anatomical single-layer structures. This new system can be commercially augmented by simultaneously capturing the 2-D OCT image and the real image of the surgical field during surgery.

2. Materials and methods

2.1 OCT system description

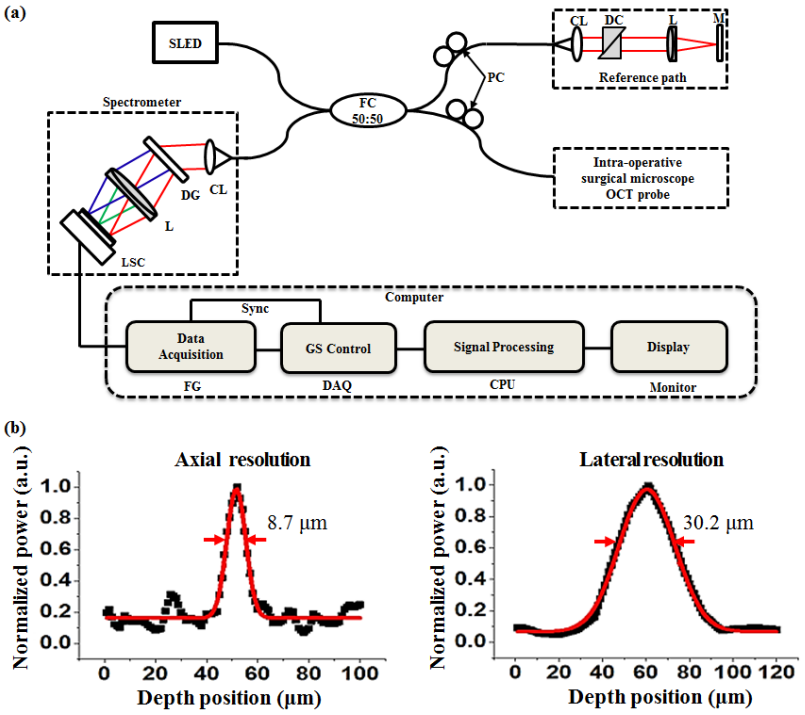

Fig. 1. Schematic and resolution of the real-time SD-OCT. (a) Schematic diagram of the real-time SD-OCT system. Abbreviations: SLED, superluminescence diode; FC, fiber coupler; PC, polarization controllers; CL, collimator; DC, dispersion compensation unit (prism pair); L, lens; M, mirror; DG, diffraction grating; LSC, line-scanning camera; Sync, synchronization; FG, frame grabber; DAQ, data acquisition board; CPU, central processing unit. (b) Measured point spread function of axial resolution at 50 μm and lateral resolution at 60 μm from zero-depth position, respectively.

#205660 - $15.00 USD Received 30 Jan 2014; revised 20 Mar 2014; accepted 21 Mar 2014; published 7 Apr 2014

A schematic diagram of the OCT system is shown in Fig. 1(a). A 12-bit complementary metal–oxide–semiconductor (CMOS) line-scanning camera (AVIIVA EM4 2048 pixels, E2V) with an effective line rate of 70,000 lines/s in 2048-pixel mode was used as the detector of the SD-OCT system. The transmission-type diffraction grating (spatial frequency: 1,800 lpmm, nominal AOI/AOD: 46.05°, Wasatch Photonics) was adapted to enhance the light efficiency in the detection path. The source was a superluminescent diode (SLED) operating in high-power mode (SLD-35-HP, Superlum, Ltd). The SLED has a center wavelength of ~870 nm and a spectrum with a full width at half maximum (FWHM) of ~65 nm. The SLED was connected to one end of a 2 × 2 (50:50) fiber-fused coupler (FC850-40-50-APC, Thorlabs). A fiber-based Michelson interferometer was implemented. The SLED was split into sample and reference paths terminated by a stationary mirror. One of the output ports was used as the reference path for animal-ear imaging and also contained a dispersion compensation unit (prism pair) to account for the dispersion within the optics of the sample path. The other output port was used as the OCT probe combined with a surgical microscope. The SLED power measured after the objective lens (an achromatic lens with a focal length of 75 mm) was ~6 mW. The developed system is experimentally determined by imaging. The detected OCT signals were transferred to a host memory in a computer mounted with four CPUs (Core 2 Quad Q8200, 2.33-GHz clock rate, Intel) through a frame grabber (PCIe-1433, 850-MB/s bandwidth, National Instruments) over two camera-link cables. A galvanometer scanner was driven by the computer with a data acquisition board (PCIe-6321, National Instruments) that can provide two analog outputs. To generate the depth-resolved sample reflectivity or A-line, the interferogram was transformed by k-domain linearization, which was completed using full-range k-domain linearization [22]. The magnitude of the fast Fourier transform (FFT) was computed. Real-time, high-resolution OCT imaging is possible with this system at a display speed of faster than 250 kHz A-scan rate, and the software used was written in LabVIEW (LabVIEW 2011, National Instruments). Figure 1(b) shows the point spread function for the axial resolution and lateral resolution, respectively. The axial resolution was measured to be ~8.7 μm in air an imaging depth position of 50 μm from the zero-depth position. The lateral resolution was measured to be ~30.2 μm from the zero-depth position. The system sensitivity was approximately 82 dB near zero optical delay when the camera was set at an exposure time of 14.1 μs. The theoretical sensitivity was approximately 96 dB because the ideal efficiency of the spectrometer was 73%, and the power at the sample path was 1.8 mW. The sensitivity of the developed system was lower than the theoretical value, mainly because of the insertion loss (−10.6 dB) between the fiber optics and the 2-D galvanometer scanner in the sample path. Losses in the other optical parts further reduced the sensitivity (−3.4 dB).

2.2 Description of the combined surgical microscope with OCT

Figure 2(a) shows the schematic diagram of the combination of the surgical microscope with OCT. We developed a real-time intraoperative surgical-microscope OCT probe combined with a commercial surgical microscope (Carl Zeiss, OPMI). The probe consisted of four subsystems: (1) the eyepiece of the surgical microscope, (2) the augmented-reality display, (3) the beam splitter mount, and (4) the OCT sample path subsystems. Figure 2(b) shows a photograph of the real system used in this study. Subsystem (1) was composed of a stereo binocular eyepiece. A monocular eyepiece (left eyepiece) played a role in the augmented reality and projected the acquired OCT images back onto the field of view (FOV) of the conventional microscope through the overlapping microscopic ocular lens. The other eyepiece (right eyepiece) acquired microscope images. Subsystem (2) was composed of a beam projector (Optoma, PR320) and two mirrors to control the beam path. If the brightness of the projected image was too high for comfortable observation with unprotected eyes, an absorptive ND filter (NE02B, Thorlabs) with a 2.0 optical density was used to reduce the brightness to an appropriate level. A variety of absorptive ND filters, which exhibit an additive relationship, were available to produce a customized level of brightness. Subsystem

#205660 - $15.00 USD Received 30 Jan 2014; revised 20 Mar 2014; accepted 21 Mar 2014; published 7 Apr 2014

(3) is a custom design, and a mount was attached to the commercial surgical microscope that held the beam splitter. A Zeiss beam splitter with a 50% reflection ratio was used in the system to reflect the augmented-reality beam to the eyepieces of the microscope. Subsystem (4) was composed of a collimator (F260APC-B, Thorlabs), 2-D galvanometer scanners (GVS001, Thorlabs), an objective lens (AC254-075-B, Thorlabs), and a dichroic mirror (NT55-233, Edmund Optics). The dichroic mirror (near infrared: 90% of reflection, visible light: 85% of transmission) was designed to reflect the 750 nm–1125 nm beam (i.e., the OCT beam) and transmit the 425 nm–675 nm beam (i.e., the surgical microscope). Further, 90% of the reflected OCT beam was transmitted via the dichroic mirror and sample.

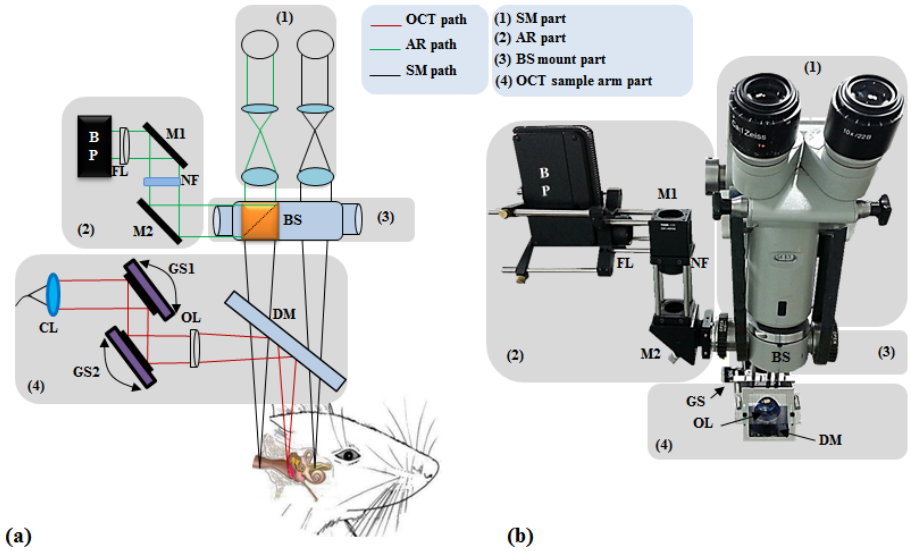

Fig. 2. (a) Schematic of a real-time intraoperative surgical-microscope OCT probe. *Abbreviations*: AR, augmented reality; SM, surgical microscope; BP, beam projector; FL, focus lens; M1, M2, mirror; NF, neutral-density filter; BS, beam splitter; CL, collimator; GS1, GS2, galvanometer scanner; OL, objective lens; DM, dichroic mirror. (b) Photograph of the real-time intraoperative surgical microscope OCT probe.

2.3 Animal preparation

The animal experiments were conducted in accordance with the guidelines of the Institutional Animal Care and Use Committee of Kyungpook National University. A total of five mice (24–28 days old, 15–30 g) without evidence of middle-ear infection were used. The animals were anesthetized by intramuscular injection using a mixture of tiletamine/zolazepam (1.8 mg/100 g) and xylazine hydrochloride (0.7 mg/100 g). After local injection of 2% lidocaine HCI and epinephrine (1:100,000), a postauricular skin incision was performed. For the *in vivo* experiment, we first positioned the mouse on its side with the left-ear incision. After making the incision, the head of the mouse was rotated counterclockwise until the malleus, incus, and stapes complex of the middle ear was visible through the opening in the bulla. We then tilted and rotated the mouse to view the apex of the cochlea. To acquire an image of the entire TM, the auricle and cartilaginous external auditory canal were removed, and the bony external auditory canal was widened by drilling. A small hole was gently drilled into the squamous bulla wall and widened to expose the round window niche and promontory. The TM was carefully removed with the ossicles intact, and the bony rim of the external auditory canal was drilled until the entire cochlea was visible by the microscope view. For realizing the hearing-loss surgery model, effusion and perforation models of chronic otitis media (OM) were simulated, which are the most common surgery models in the OM.

#205660 - $15.00 USD Received 30 Jan 2014; revised 20 Mar 2014; accepted 21 Mar 2014; published 7 Apr 2014

3. Results

3.1 In vivo imaging of the TM and middle-ear structure

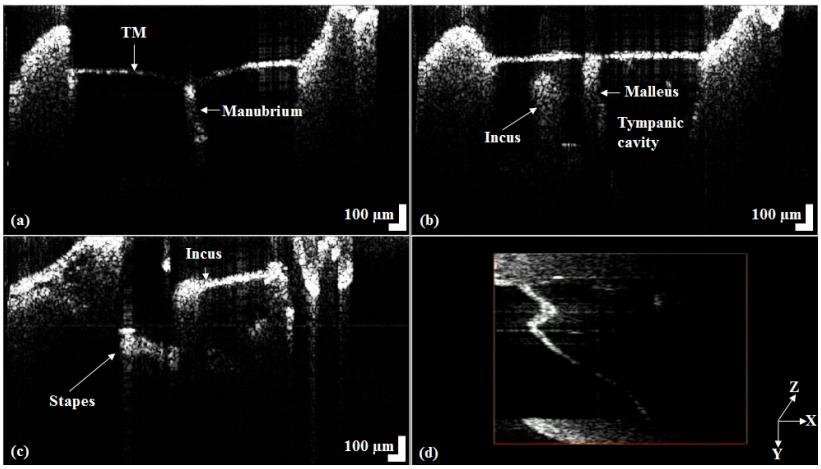

Fig. 3. Images of an *in vivo* 2D mouse TM and middle-ear structure: (a) including the TM connected to the upper middle ear, (b) including the ossicles part (malleus and incus) and tympanic cavity of the middle ear, (c) cochlea connected part (incus and stapes) of the lower middle ear, and (d) 2-D movie of the whole middle-ear structures (Media 1).

Figure 3 shows the 2-D tomographic images of the TM and middle ear. Figure 3 (a) includes the manubrium, which connects the TM and the ossicles with the top part of the TM and middle ear. Figure 3(b) shows the tympanic cavity of the ossicles, including the malleus and incus, which transmit vibration from the outer ear to the center of the middle ear through the TM. Figure 3(c) shows the structure of the stapes and incus, which transmit vibration from the middle ear through the inner ear to the cochlea. In Media 1, 2D X-Y and Y-Z side views of the whole middle-ear structures are shown. Figure 3(d) shows a screenshot from Media 1 that shows the configuration of the 2-D images of the middle ear including the TM. The resolution of the image from the SD-OCT system is 1,024 × 500. The FOV of the back-projected OCT B-scan was approximately 3 mm × 3 mm along the X and Y axes, respectively.

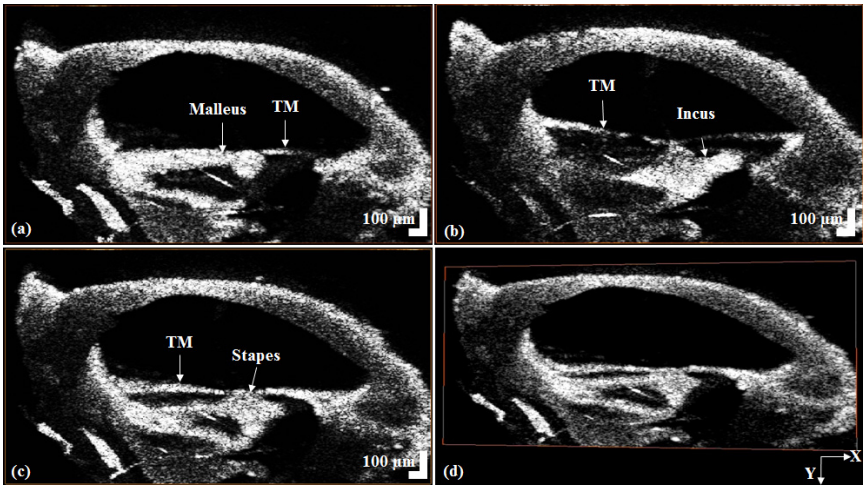

Fig. 4. Images of an *in vivo* 3D mouse TM and middle-ear structure: (a) including the TM connected to the upper middle ear, (b) including the ossicles part (malleus and incus) and the tympanic cavity of the middle ear, (c) cochlea-connected part (incus and stapes) of the lower middle ear, and (d) 3D en-face movie of the whole middle-ear structures (Media 2).

#205660 - $15.00 USD Received 30 Jan 2014; revised 20 Mar 2014; accepted 21 Mar 2014; published 7 Apr 2014

Figure 4 shows - the2-D cross sectional images from the top-view of the malleus, incus, and stapes of the ossicles in the Tm and the middle ear which constructs the 3-D image. Figure 4(a) shows the microstructure of the malleus located on the top part of the TM and ossicles, and Fig. 4(b) shows the TM and incus microstructure, which is located in the middle of the malleus and stapes of the ossicles. Figure 4(c) shows the fine microstructure of the TM and stapes, which connects with the cochlea of the inner ear located at the bottom part of the ossicles. Media 2 is a 3D en-face movie of the whole middle-ear structures. Figure 4(d) shows the entire 3-D image of the middle ear including the TM from the en-face Media 2. The components of the fine microstructures of malleus, incus, and stapes of the ossicles and TM can be identified using the depth images acquired by OCT.

3.2 In vivo imaging of the whole ear structure

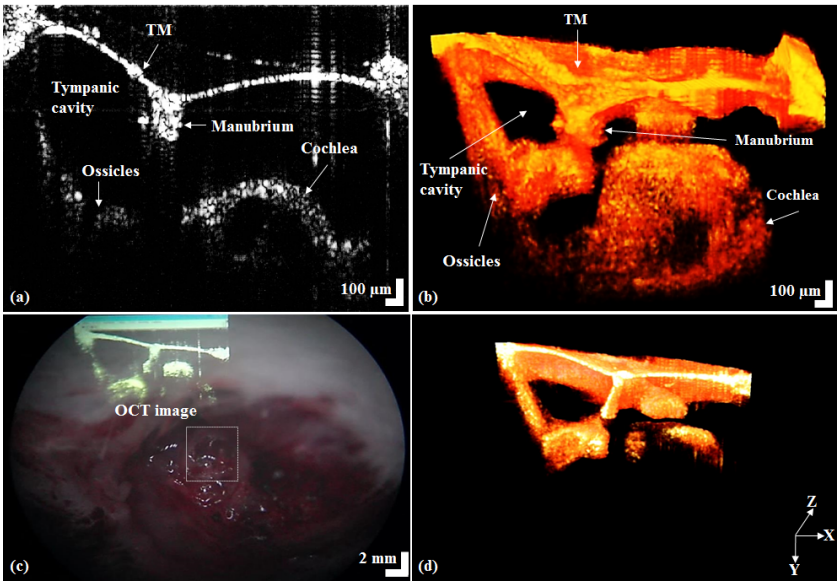

Fig. 5. *In vivo* whole mouse-ear structural images using OCT combined a surgical microscope. (a) 2-D image of the whole ear structure. (b) 3-D image of the whole ear structure. (c) Using the AR image of the combined OCT and surgical microscope system obtained via the left eyepiece during 3-D imaging for the whole ear structure. The rectangle box represents the scanning area. (d) 3-D movie of the whole ear structure (Media 3).

Figure 5 shows the whole structure of the mouse ear, and the cochlear structure of the inner ear along with the middle ear including the TM. Figure 5(a) shows the 2-D image of the top surface of a single-layer structure starting from the TM, manubrium, tympanic cavity, ossicles, and cochlea. Figure 5(b) shows a reconstructed 3-D image using the 2-D OCT images in Fig. 5(a). Media 3 shows the whole ear structure using the AR images of the combined OCT and surgical microscope obtained via the left eyepiece during 3D imaging. Figure 5(c) shows a screenshot acquired via the left eyepiece during 3-D scanning of the whole mouse ear. A 2-D cross-sectional OCT image was superimposed with the surgical-microscope image for simultaneous observation. The overlapped image could be observed through the left eyepiece of the surgical microscope. Media 3 shows the 3-D OCT images of the X-Y side view of the whole mouse structures. Figure 5(d) shows a clear microstructure of a mouse TM, middle ear, and cochlea of the inner ear, as confirmed in Media 3.

#205660 - $15.00 USD Received 30 Jan 2014; revised 20 Mar 2014; accepted 21 Mar 2014; published 7 Apr 2014

3.3 In vivo imaging of the apex of the cochlear structure

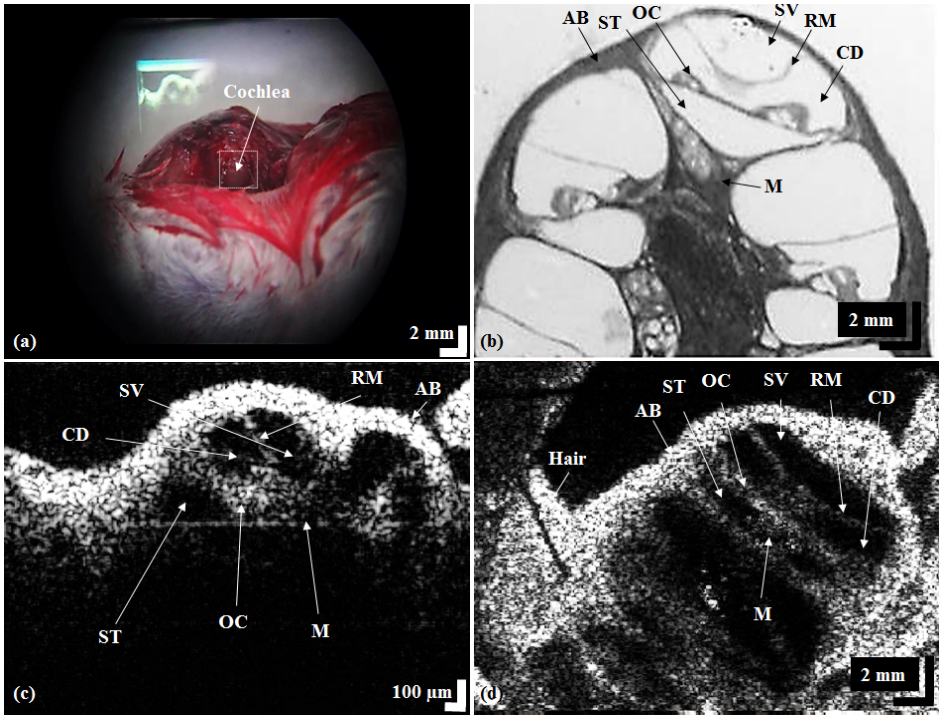

Fig. 6. *In vivo* inner-ear structure images of a mouse using OCT combined with a surgical microscope. (a) Using the AR image of the combined OCT and surgical-microscope images obtained via the left eyepiece during 3-D imaging of tiny structures of the cochlea. The rectangle box represents the scanning area. (b) Histologic image of a cochlear cross section. (c) 2-D image at the apex of the tiny cochlear structures (Media 4). (d) 3-D en-face movie at the apex of the tiny cochlear structures (Media 5). *Abbreviations*: AB, Apex bone; ST, Scala tympani; OC, Organ of Corti; SV, Scala vestibuli; RM, Reissner's membrane; CD, Cochlear duct; M, Modiolus.

Figure 6 shows the apex images of the inner ear of the mouse cochlea. Figure 6(a) shows the apex image acquired via the left eyepiece for the mouse inner ear. Figure 6(b) shows a histology image of the apex of the cochlear cross section at a position similar to the OCT image. Figure 6(c) shows the *in vivo* 2-D OCT cross-sectional image, which is an apex of the cochlea imaged through the intact apex bone. Figure 6(d) shows screenshots of intact cochlear intrastructures. Figures 6(b)-(d) show that the bony labyrinth of the cochlea has a spiral shape similar to the space inside a snail shell. The cochlea consists of relatively large fluid-filled spaces referred to as the scala vestibuli (SV), cochlear duct (CD), and scala tympani (ST). Furthermore, the OCT imaging method is able to detect a wide variety of tissue types ranging from acellular gelatinous material (Reissner's membrane) to dense bone (the apex bone) to the epithelial organ of Corti, which contains remarkably delicate hair cells. For a better view of the cochlear microstructure, the 3-D *in vivo* en-face OCT images from the apex to the medial turns are shown in Media 5.

#205660 - $15.00 USD Received 30 Jan 2014; revised 20 Mar 2014; accepted 21 Mar 2014; published 7 Apr 2014

3.4 In vivo imaging of the conductive hearing-loss model

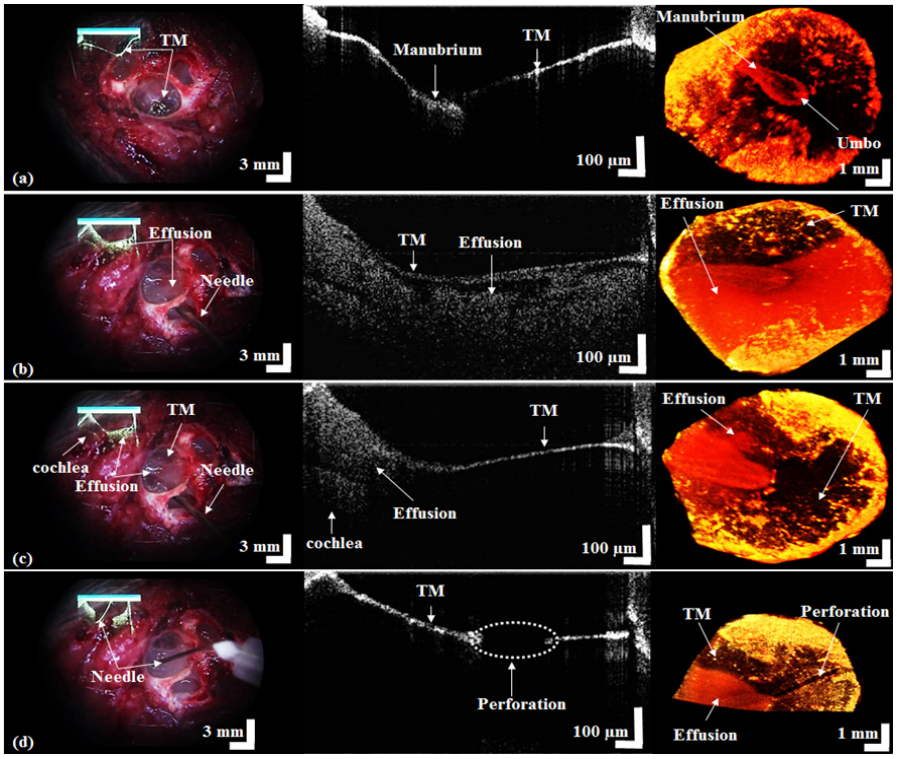

Fig. 7. Screenshots of real-time AR using OCT combined with a surgical microscope for the *in vivo* intraoperative conductive hearing-loss model of a mouse. The line represents the scanning area. (a) Normal TM images of AR using OCT combined with a surgical microscope, 2-D OCT image, and 3-D en-face image (Media 6). (b) Effusion injection of the OM model (Media 7). (c) Suction of the effusion OM model (Media 8). (d) Included perforation of the chronic OM model (Media 9).

Figure 7 shows an image obtained after the experiment considering the surgical environment of the hearing-loss model. Surgical-microscope, 2-D OCT, and 3-D images for the normal, effusion OM, and chronic OM models were obtained by using the AR-based surgical microscope combined with OCT for the same mouse. Figure 7(a) shows a screenshot from Media 6 acquired via the left eyepiece when the whole TM of the mouse is scanned in 3-D for the normal model. The TM is clear in the surgical microscope, and the normal TM structure is also clearly observed in OCT images as well. Even in the 3-D image, a manubrium and umbo structure that connects the TM and ossicles can be seen clearly. Media 7 show an effusion injection for the effusion OM model. From Fig. 7(b), injection of the effusion into the tympanic cavity of the bottom part of the TM can be seen in the AR surgical-microscope OCT image. The 2-D OCT image shows that the injected effusion is visible in the gap between the tympanic cavity and the cochlea. In addition, some distinct fine particles from TM organization can be confirmed by considering the 3-D images. The suction process of the effusion is shown in Media 8. The 2-D and 3-D OCT images in Fig. 7(c) show that the effusion remains despite the suction. Thus, the effusion remains in the tympanic cavity and cannot be recovered, even if effusion removal surgery is carried out. Therefore, this indicates a need for tympanostomy tube surgery [23]. As shown in Media 9, the TM perforation was reproduced for realizing the chronic OM model when the tympanic cavity is in the full state with the effusion. Even though the TM perforation cannot be seen clearly in the surgical-microscope view in Fig. 7(d), the 2-D OCT image provides a clear view of it. Further, the size

#205660 - $15.00 USD Received 30 Jan 2014; revised 20 Mar 2014; accepted 21 Mar 2014; published 7 Apr 2014

and shape could be clearly confirmed via 3-D OCT. We could apply the developed system to the intraoperative surgery in otolaryngology thorough this experiment. The utility of the intraoperative hearing loss in otolaryngology was amply confirmed through this experiment.

4. Discussion

Herein, we demonstrated various experiments to confirm the suitability of this method for otolaryngology. First, the feasibility of using AR OCT combined a surgical microscope for clear visualization of a living mouse TM, middle-ear microstructures (malleolus, incus, stapes), and inner-ear (cochlear) micro-anatomical features was successfully demonstrated. The developed system that provides *in vivo* high-resolution imaging to reveal anatomic and physiological information of the middle ear and inner ear in a relatively noninvasive and nondestructive manner might shed light on the fundamental issues concerning hearing function and loss, enable clinically significant diagnoses, and guide surgical efforts to restore hearing function by an intraoperative surgical microscope. The first results of the current study of *in vivo* imaging of middle-ear microstructures and inner-ear structure morphology with SD-OCT suggest that this imaging method deserves exploration for otology applications. As a reference during surgery, CT and MRI are often utilized for entire-body ear imaging prior to surgery. Due to their limited resolution as 50 um and 100 um, respectively, microstructural visualization of the entire-body ear is not feasible. Also, these modalities have limitation in being used as a real-time feedback imaging modalities during surgery. Because the proposed method feedbacks the live OCT images onto the ocular lens of the surgical microscope, surgeon has no need to look away from the microscope view to the OCT display. So, it can be used as a live reference in intraoperative procedure. In addition, we realized the hearing-loss surgery model of a living mouse to confirm the suitability of the developed system for identifying the detailed tiny structures. A normal model, an effusion OM model, and complex diseases of effusion and the TM were utilized to perform experiments using AR OCT combined with a surgical microscope. The results were confirmed as real-time AR images by overlapping the 2-D OCT image with the microscope image, which was obtained through the left eyepiece of the surgical microscope. These results verify the usefulness of this method for otolaryngology surgeries and also confirm that the 3-D images are comparatively clearer than conventional microscope images. In addition, the perforations that cannot be viewed using a surgical-microscope view can be confirmed using the OCT image of the AR using the combined OCT and surgical-microscope views in real-time. Therefore, it is confirmed that the enhanced method is suitable owing to the capability of real-time verification during an actual hearing-loss intraoperative surgery. As discussion of the challenges and limitations of the augmented reality presentation of OCT, the working distance from the objected lens to the surgical site should be sufficiently maintained for surgeon's operation. If the distance is too short, it may limit the surgeon's hand movement. However, there is a tradeoff in lengthening the distance by sacrifice the lateral resolution of the OCT image. One needs to note that OCT image in this approach is mainly for monitoring the surgical site in depth, not for pathological diagnosis. Sacrifice of the lateral resolution may be more endurable. Another issue to consider is the position of the augmented reality display. Flexible relocation as the user's preference may be significantly helpful in an intraoperative environment. Real-time three dimensional OCT display would be also an important improvement to increase the efficacy of this approach.

5. Conclusion

In this study, we developed a system that combines a surgical microscope with OCT using AR. OCT 2-D and 3-D images of the developed system confirm the middle-ear and inner-ear structures of a live mouse. The developed system is different from the conventional method, as the monolayers of each microstructure can be viewed in real-time without the aid of any foundry molding preparation. To the best of our knowledge, this is the first demonstration of

#205660 - $15.00 USD Received 30 Jan 2014; revised 20 Mar 2014; accepted 21 Mar 2014; published 7 Apr 2014

overlapping *in vivo* animal real-time imaging of whole middle-ear and inner-ear tiny morphology and intraoperative surgery using the AR OCT combined surgical microscope.

Acknowledgments

This work was financially supported by a grant from the Korea Healthcare Technology R&D Project, Ministry of Health & Welfare, Republic of Korea (A102024-1011-0000200), "Over regional linked 3D convergence industry promotion program" through the Ministry of Trade, Industry & Energy (MOTIE) and Korea Institute for Advancement of Technology (KIAT) (No. R0001512), and the National Institutes of Health (No. 201225940000).

#205660 - $15.00 USD Received 30 Jan 2014; revised 20 Mar 2014; accepted 21 Mar 2014; published 7 Apr 2014